Investigation into the magnetic properties of CoFeNiCryCux alloys

James Harris, Zhaoyuan Leong, Peng Gong, Juan Cornide, Charlotte Pughe, Thomas Hansen, Aris Quintana-Nedelcos, M. Calvo-Dahlborg, Richard Rowan-Robinson, Ulf Dahlborg, et al.

Investigation into the magnetic properties of $CoFeNiCr_yCu_x$ alloys

Investigation into the magnetic properties of $CoFeNiCr_yCu_x$ alloys

James Harris[1], Zhaoyuan Leong[1], Peng Gong[1], Juan Cornide[2,3], Charlotte Pughe[1], Thomas Hansen[4], Aris Quintana-Nedelcos[1,5], Richard Rowan-Robinson[1], Ulf Dahlborg[3], Monique Calvo-Dahlborg[3], Russell Goodall[1], Mark Rainforth[1] and Nicola Morley[1*]

[1]Department of Materials Science and Engineering, University of Sheffield, Sheffield, S1 3JD, UK

[2]Department of Materials Science and Engineering and Chemical Engineering, Universidad Carlos III de Madrid, Avda. Universidad 30, Leganés, 28911, Spain

[3]Groupe de Physique des Materiaux, UMR 6634, University Rouen Normandie, Campus Madrillet, B.P. 12, 76801 Saint-Etienne de Rouvray Cedex, France.

[4]Intitute Laue-Langevin, 71 Avenue des Martyrs, 38000 Grenoble, France

[5]New Model Institute for Technology and Engineering, Gardner Hall, Venns Lane, Hereford, HR1 1DT, UK

*****Corresponding Authors email: n.a.morley@sheffield.ac.uk

Abstract

The search for cheap, corrosion-resistant, thermally-mechanically stable functional magnetic materials, including soft magnetic and magneto-caloric materials has led to research focused on high entropy alloys (HEAs). Previous research shows that alloying elements with negative enthalpies of mixing can facilitate a second-order phase transition. On the other side of the spectrum, compositional segregation cause by positive enthalpy of mixing alloying additions (such as Cu) may also be used to tune magnetic properties. This paper studies the structural, magnetic and magneto-caloric effect of the FCC alloys $CoFeNiCr_yCu_x$ (x = 0.0, 0.5, 1.0 and 1.5, y = 0.0, 0.8 and 1.0) to tune these properties with Cu and Cr alloying. Scanning electron microscopy (SEM) of the compositions show nanoparticles forming within the grains as the Cu concentration increases. Cr addition to $CoFeNiCu_{1.0}$ has a larger effect on the magnetic and magneto-caloric properties compared to the Cu addition to $CoFeNiCr_{1.0}$. The addition of Cu (x

= 0.5) to $CoFeNiCr_{1.0}$ improved both the saturation magnetisation and Curie temperature; addition of Cr (y = 1.0) to $CoFeNiCu_{1.0}$ decreased the Curie temperature by 900 K. All alloys were determined to have a second-order phase transition around their Curie temperature. The refrigerant capacity at 2 T was found to be similar to existing HEAs, although the Curie temperatures were lower than room temperature. Based on this data the $CoFeNiCr_{0.8}Cu$ composition was fabricated to increase the Curie temperature towards 300 K to explore these HEAs as new candidates for room temperature magneto-caloric applications. The fabricated composition showed Curie temperature, saturation magnetisation, and refrigerant capacity increasing with the small reduction in Cr content.

Keywords: Multi-component alloys; Soft Magnetic; Magneto-caloric; Microstructure; Magnetisation; High entropy alloys

1. Introduction

Modern developed life relies on refrigeration for many reasons including: preserving food, controlling the environment of homes or workplaces, and freezing medical samples. This creates a huge demand for energy. In developed countries; half of the EU energy consumption is for the purpose of controlling temperature through heating or cooling [1]. Furthermore, much of this energy is wasted. In the UK, only 37% of energy was used in useful energy applications in 2011, leaving a huge energy waste of 63% [2]. Reducing this waste will help to lower emissions, reduce dependency on energy imports in some countries, and cut costs for households and businesses. An estimated 87% of US households have air conditioners. Collectively this accounts for around 186 billion kWh of electricity every year [3]. This energy inefficiency coupled with a high demand for refrigerating devices creates a need for lower energy refrigeration technologies, which are more efficient than the current vapour gas cycle. One such method uses the magneto-caloric effect (MCE), the reversible temperature change of a magnetic material when an external magnetic field is applied in adiabatic conditions [4].

The search for a suitable magneto-caloric material has branched out from Gd based materials into La(Fe, Mn, Co, Mn)$_{13-x}$Si$_x$(H, N,C)$_y$ [5,6], MnAs$_{1-x}$Sb$_x$ [7], Fe_2P style materials [8], as well as Ni-Mn based Heusler alloys, which have a Heusler structure and composition XYZ, with X and Y being transition metals and Z a P block element [9], and $La_{1-x}Ca_xMnO_3$ manganites [10], among others. These magneto-caloric materials can be tuned so that their Curie temperature (T_c) is around 250 - 300 K to allow for room temperature refrigeration. The main disadvantages are that the materials either contain expensive rare earth elements (LaFeSi) or toxic elements (MnAsSb) or have poor mechanical properties (Heusler alloys). Therefore, the search for new magneto-caloric materials to replace current cooling technology demands the material has not only attractive magneto-caloric properties such as a wide temperature range and low hysteresis losses, but also satisfies requirements of any household device such as good corrosion resistance, good mechanical properties, and non-toxic (or does not break-down into toxic components).

A suggested route to achieve this is the investigation of high entropy alloys (HEAs), a subset of multi-component alloys (MCAs). This is due to their excellent mechanical and corrosion resistant properties, being close to those of austenitic and ferritic stainless steels. In a review of magneto-caloric materials, Gutfleisch *et al*. [11] suggested the ideal magnetic material

would contain 80% transition metals with large magnetic moments such as Fe and Mn and inexpensive P band metals such as Al or Si. They also suggested other requirements including: magnetic ordering transitions of first order, workability like that of steel, corrosion resistance similar to stainless steel and a high electrical resistance. Properties and features similar to these have been reported in HEAs, such that a few research groups have already investigated the magneto-caloric effect (MCE) in HEAs. Kurniawan *et al.* [12], were the first to put forward HEAs as possible low-cost MCE materials. They studied how the Curie temperature of FeCoNiCuMn could be tuned to be around 300 K, by changing the ratio of Cu to Mn. While Calvo-Dahlborg *et al.* found that the magnetic transition temperature can be tuned to be around room temperature with either FCC or BCC structure with a Hume-Rothery approach based on *e/a* and atomic radius [13]. Belyea *et al.* [14] studied magneto-caloric effects in $NiFeCoCrPd_x$. They found that by changing the amount of Pd within the alloy they were able to tune the Curie temperature from room temperature down to 100 K, while maintaining a refrigerant capacity of around 50 J/kg at 2 T. Lucas *et al*. [15] studied the structural and magneto-caloric properties of cold-rolled $FeCoNiCr_x$ alloys after different heat treatments. They found that all the $FeCoNiCr_x$ alloys studied had a FCC structure. They also found decreasing the Cr concentration increased the Curie temperature, but did not change the magnetic entropy change (ΔS_m) value. The main difference between the heat treated and cold-rolled samples was that the heat-treated samples had a narrow operational temperature range, thus a smaller refrigerant capacity. For the FeCoCrNi alloy at 1.5 T and 100 K, the refrigerant capacity was 43 J/kg. Na *et al*. [16] studied the structural, magnetic and magneto-caloric properties in the HEA FeCoNiCrAl. They changed the ratio of Ni to Cr within the alloy, and found that the structure changed from single phase BCC for 1:1 ratio to a mixed BCC and FCC phase for 1.5:0.5 ratio. The FeCoNiCrAl alloy had a Curie temperature of 290 K and a refrigerant capacity of 119 J/kg at 3 T, demonstrating their promise for room temperature magnetic refrigeration. Quintana-Nedelcos *et al.* [17] studied the MCE of the dual phase alloy $CoFeNi_{0.5}Cr_{0.5}Al_x$, and determined that the refrigerant capacity seemed to be independent of the composition, as both the x = 0.0 (single phase, FCC, T_c = 270 K) and x = 1.5 (dual phase, BCC, T_c = 465 K) had a refrigerant capacity of 75 J/kg at 2 T. Although lower than the traditional first order MCE materials, so not as competitive for magneto-refrigeration, other applications such as thermal energy harvesting from waste heat are also options. One advantage of HEAs is that although there is a magnetic property-Curie temperature trade off, this can be

mitigated by balancing the stoichiometry through changes in one or two of the elements. In this way the magnetic and magneto-caloric properties can be maintained. [12-17]. This is advantageous for applications such as magnetic refrigeration and thermal energy harvesting, as it allows for a graded component to be produced that will operate over a wide temperature range, without too much loss in refrigerant performance.

The HEA CoFeNiCrCu has been studied previously to understand its structural, mechanical, high temperature and corrosion resistance [18-22]. Praveen *et al*. [18] studied the alloying behaviour in NiCoCrCuFe alloys. They found that before milling CoFeNiCu, CoFeNiCr and CoFeNiCrCu all had one FCC phase, with CoFeNiCu and CoFeNiCrCu retaining the FCC phase after milling but with the addition of a BCC phase. They also found that the Vickers hardness was largest in the CoFeNiCr sample compared to the CoFeNiCrCu and CoFeNiCu samples, meaning the Cr is required to achieve a high hardness. Guo *et al.* [19] studied a series of CoNi based alloys (CoNi, CoFeNi, CoCrFeNi and CoCrCuFeNi) to understand how the single FCC phase solid solutions were formed. They found that there was a critical lattice distortion with the addition of both Cr and Cu to CoFeNi, with a second FCC phase occurring in the CoCrCuFeNi alloy. Dahlborg *et al.* [20] investigated the crystalline structure of CoFeNiCr with the addition of Pd, Sn and Cu. They determined that CoFeNiCr is single phased FCC, while CoFeNiCrCu contains three FCC phases, one with the same lattice constant as Cu, one with a similar lattice constant to CoFeNiCr and a third, which is smaller than both. Verma *et al.* [21] studied how the Cu concentration in CoFeNiCr changed the microstructure and the wear resistance. They found that CoFeNiCr has a single FCC structure, but as the Cu concentration increases, two FCC structures appear, due to the segregation of Cu into the grain boundaries. The increase in Cu also increases the hardness, so decreasing the wear rate. Muangtong *et al.* [22] investigated the corrosion behaviour of CoFeNiCr with the addition of Cu, Al or Sn. They found that CoFeNiCrSn and CoFeNiCr had corrosion resistance better than steel.

While the structural phases and wear resistance of these materials are now well known, less is known about their magnetic and magneto-caloric properties. Therefore, to improve understanding of the material properties and determine the effect of the Cr to Cu ratio, this work studied the HEA $CoFeNiCr_yCu_x$, where $0 \leq y \leq 1$ and $0 \leq x \leq 1.5$. Whilst improving our understanding of material properties, this research allows assessment of whether tuning the

composition of $CoFeNiCr_yCu_x$ has the capability to achieve a competitive refrigerant capacity at room temperature.

2. Experimental Procedure

The HEAs investigated in this paper were $CoFeNiCr_yCu_x$, x = 0.5, 1.0 and 1.5 and y = 0.0, 0.8 and 1.0. To avoid confusion between the different alloys, a simpler notation for each alloy is used: CFN-Cr_yCu_x. The alloys studied by varying the Cu concentration were: CFN-$Cr_{1.0}Cu_{0.0}$, the CFN-$Cr_{1.0}Cu_{0.5}$, CFN-$Cr_{1.0}Cu_{1.0}$, and CFN-$Cr_{1.0}Cu_{1.5}$ and varying the Cr concentration: CFN-$Cr_{0.0}Cu_{1.0}$, CFN-$Cr_{0.8}Cu_{1.0}$, and CFN-$Cr_{1.0}Cu_{1.0}$ (see Table 1). The CFN-$Cr_{1.0}Cu_{0.0}$ alloy has previously been studied [20], so the results are compared with the new alloys. The samples were fabricated via arc-melting, using elements with at least 99% purity. The elements were melted in a copper hearth, which was cooled by water and under an argon atmosphere. The ingots were remelted at least three times to ensure homogenous mixing. The samples were then suction cast into 3 mm rods, in a copper mould cooled by water.

For the CFN-$Cr_{1.0}Cu_x$ samples, X-Ray Diffraction (XRD) using a Stoe Stadi P instrument in transmission XRD mode was used. The radiation source used was Mo (K_α wavelength = 0.71 Å), to determine the phases present in the samples and to avoid fluorescence effects. For the CFN-$Cr_yCu_{1.0}$ samples, the rasped powders were loaded into a cylindrical sample holder and the XRD pattern measured using a Rigaku Miniflex diffractometer, with Cu source (K_α wavelength = 1.54 Å). Room temperature (298 K) diffraction patterns were then collected using a 2ϑ(°) range of 30-100°, encompassing the major reflections. To further investigate the phases, neutron diffraction measurements were carried out at the Institut Laue-Langevin (ILL), France on the D20 diffractometer for the CFN-$Cr_{1.0}Cu_{0.0}$, and CFN-$Cr_{1.0}Cu_{1.0}$ samples. The wavelength of the incident neutrons was 1.12 Å with a maximum measured wave-vector transfer of 10.8 $Å^{-1}$. From both sets of data, the crystal structure, and lattice constants were determined. From the XRD data, the crystallite size and strain were determined using the Williamson-Hall (WH) method.

The composition of each sample was measured on a Scanning Electron Microscope (SEM) using Energy Dispersive X-ray (EDX). Composition results are given in Table 1. The compositions measured were in good agreement with the target compositions, indicating there was very limited loss of the elements during the processing. Specimens for SEM

observation were prepared by standard metallographic methods, which included grinding from P400 to P1200 and polishing down to 0.04 µm colloidal silica particles. SEM for microstructure observation was undertaken using Inspect F50, FEI in backscattered electron (BSE) mode with EDX for elemental detection on the specimen surface.

The magnetic properties were measured using a MPMS-3 SQUID-VSM magnetometer. For the samples containing Cr, the magnetic hysteresis loops were measured at 300 K and 10 K, to determine the magnetic behaviour, along with the saturation magnetisation, if they were ferromagnetic. Zero-field cooled (ZFC) and field cooled (FC) temperature measurements were taken to determine the Curie temperature between 350 K and 10 K. These were taken at 24 kA/m and 795 kA/m. AC susceptibility measurements were taken between 5 K and 350 K, at an applied field of 798 A/m and frequencies, 10, 100 and 1000 Hz. While first quadrant magnetisation vs magnetic field data were taken every 10 K between 350 K and 10 K for the magneto-caloric data. For the CFN-$Cr_{0.0}Cu_{1.0}$ sample, the high temperature option for the MPMS-3 magnetometer was used, with the magnetic hysteresis loops being measured at 300 K and 1000 K and the ZFC-FC temperature graphs being measured between 300 K and 1000 K. The magneto-caloric data was taken from 550 K up to 1000 K.

Table 1. Composition and structural properties of the CFN-$Cr_{1.0}Cu_x$ and CFN-$Cr_yCu_{1.0}$ samples

Sample/ Notation	**Composition (*via* EDX)**	**Phase**	**Lattice Constant (Neutron) (Å)**	**Lattice Constant (XRD) (Å)**	**Crystallite Size (WH) (nm)**	**Strain (WH)**	**Wigner-Seitz radius (Å)**
CFN-$Cr_{1.0}Cu_{0.0}$ [20]	Not Available	FCC	-	3.57	36	0.0018	1.3971
CFN-$Cr_{1.0}Cu_{0.5}$	$Co_{23}Fe_{21}Ni_{22}Cr_{22}Cu_{12}$	FCC	-	3.589	19	0.0043	1.4026
CFN-$Cr_{1.0}Cu_{1.0}$	$Co_{19}Fe_{21}Ni_{20}Cr_{22}Cu_{18}$	FCC FCC	3.589 3.548	3.591	20	0.0049	1.4034
CFN-$Cr_{1.0}Cu_{1.5}$	$Co_{17}Fe_{16}Ni_{18}Cr_{19}Cu_{30}$	FCC	-	3.596	101	0.01	1.4053
CFN-$Cr_{0.0}Cu_{1.0}$	$Co_{27}Fe_{25}Ni_{24}Cu_{24}$	FCC	3.552	3.584	13	0.0014	1.4006
CFN-$Cr_{0.8}Cu_{1.0}$	$Co_{22}Fe_{21}Ni_{21}Cu_{21}Cr_{15}$	FCC	-	3.586	24	0.0025	1.4013

3. Results and Discussion

3.1 Crystal Structure

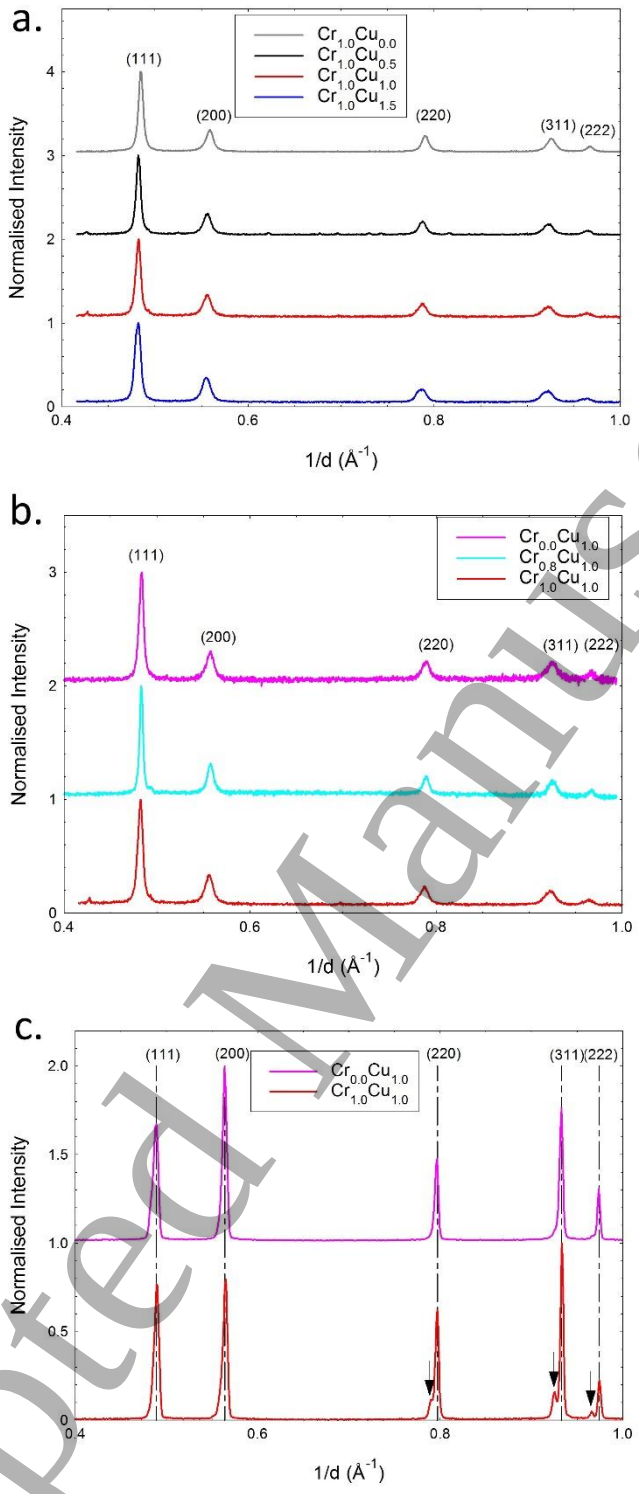

Figure 1a. XRD of the CFN-$Cr_{1.0}Cu_x$ samples. b. XRD of the CFN-$Cr_yCu_{1.0}$ samples and c. Neutron diffraction of the CFN-$Cr_{1.0}Cu_{0.0}$, and CFN-$Cr_{1.0}Cu_{1.0}$ samples. The dashed lines indicate the main FCC phase and the arrows indicate the second FCC phase. The XRD and neutron data has been normalised to the largest peak.

The XRD and neutron data are both presented as function of 1/d, to allow comparison between the two (Figure 1). The XRD data were taken for the CFN-$Cr_{1.0}Cu_x$ samples (Figure 1a) and CFN-$Cr_yCu_{1.0}$ samples (Figure 1b). For all the samples studied, the only phase was FCC. It was observed that with the increase in Cu addition, there is a broadening of the (220) and (311) peaks, which suggests that a second FCC phase occurs (Figure 1a) with $x > 1.0$. As the XRD data did not conclusively show this, neutron data for three samples (CFN-$Cr_{1.0}Cu_{0.0}$, CFN-$Cr_{1.0}Cu_{1.0}$ and CFN-$Cr_{0.0}Cu_{1.0}$) were studied. From Figure 1c. it is observed that for the CFN-$Cr_{1.0}Cu_{1.0}$ sample, there exist two FCC phases. While for the CFN-$Cr_{0.0}Cu_{1.0}$ sample, only one FCC phase exists, for the CFN-$Cr_{1.0}Cu_{0.0}$ sample, it has been widely reported in the literature to possess only the FCC phase in the as-cast state [20]. Table 1 gives the lattice constants, crystallite size and strain of the samples determined from Figures 1. The different resolution of the three diffraction techniques, *i.e.* XRD, neutron diffraction and High Energy XRD, is compared elsewhere [23].

Previous work on the addition of transition metal elements to Ni [19], has shown that the lattice constant always increases from the Ni lattice constant (3.524 Å). Cu is also FCC and has a lattice constant of 3.615 Å. From the literature, there is a range of lattice constants given for CFN-$Cr_{1.0}Cu_{1.0}$, suggesting that the lattice constant somewhat depends on the synthesis process, but not the phase, as all the literature for CFN-$Cr_{1.0}Cu_{1.0}$ gives the phase as FCC, with the lattice constant values range from 3.575 Å [20] to 3.62 Å [18]. The lattice constant for CFN-$Cr_{1.0}Cu_{0.0}$ ranges from 3.572 Å [19] to 3.59 Å [18], while CFN-$Cr_{0.0}Cu_{1.0}$ is given as 3.6 Å [18]. The lattice constants for the CFN-$Cr_{1.0}Cu_x$ alloys in this work are reported in Table 1. As expected, the lattice constant increases as the Cu concentration increases in CFN-$Cr_{1.0}Cu_x$, eventually approaching the Cu element lattice constant. All the measured values for the CFN-$Cr_{1.0}Cu_x$ alloys are within the range reported in the previous literature [18-20]. The exception is the CFN-$Cr_{0.0}Cu_{1.0}$ sample, where the lattice constant is smaller than the literature value [18]. From the Williamson-Hall (WH) plots, the crystallite size and strain can be calculated (Table 1). For all compositions studied the WH plots suggest a degree of lattice strain is present within the alloys. The strain increases as the Cu concentration increases. For the alloys with $x \leq 1.0$, the crystallite size is less than 50 nm, but is doubled for the CFN-$Cr_{1.0}Cu_{1.5}$ alloy. This may be due to the additional Cu causing two FCC phases to form.

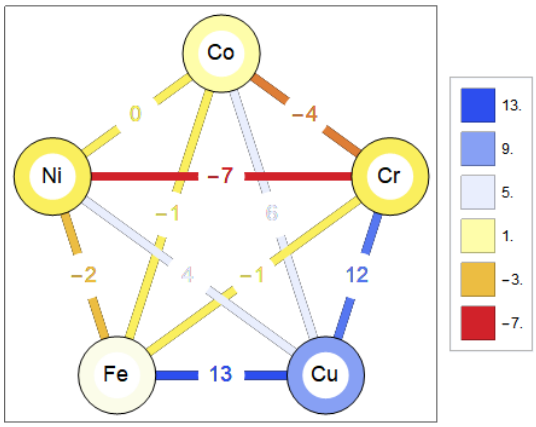

Figure 2. Enthalpy of mixing values for CFN-$Cr_{1.0}Cu_{1.0}$. The individual alloying elements are colour coded according to the average enthalpy of mixing values they have with the other compounds.

In the CFN-Cr_yCu_x compositions studied here, the elements all adopt the FCC structure. Analysis of the binary enthalpies of mixing of the alloying components suggests that CoFe (-1 kJ/mol) and CrNi (-7 kJ/mol) pairs dominate in the CFN-$Cr_{1.0}Cu_x$ alloy for all values of *x* from 0 through 1.5 (Figure 2). The addition of Cu leads to Cu segregation due to its positive enthalpy of mixing and dilution of the Co-Fe-Cr-Ni ferromagnetic elements. It is expected that some CuCo (6 kJ/mol) and CuNi (4 kJ/mol) pairs might form due to their lower enthalpies of mixing. This analysis is supported by [23] where it was inferred that the CFN-$Cr_{1.0}Cu_{0.0}$ phase is diluted by addition of Cu; similarly [24] suggests that the CFN-$Cr_{1.0}Cu_{1.0}$ composition gives rise to a CoFeNiCr-rich matrix with Cu segregation containing some Co and Ni additions, which is in agreement with our analysis. Analysis of the CFN-$Cr_{0.0}Cu_{1.0}$ composition shows that CoFe (-1 kJ/mol), CoNi (0 kJ/mol), and FeNi (-2 kJ/mol) dominates while CoCu (6 kJ/mol) and excess Cu would also be present. This suggests that the composition of the secondary phase in CoFeNiCu will be different from that of the CFN-$Cr_{1.0}Cu_x$ due to the Cr removal.

3.2 Microscopy Analysis

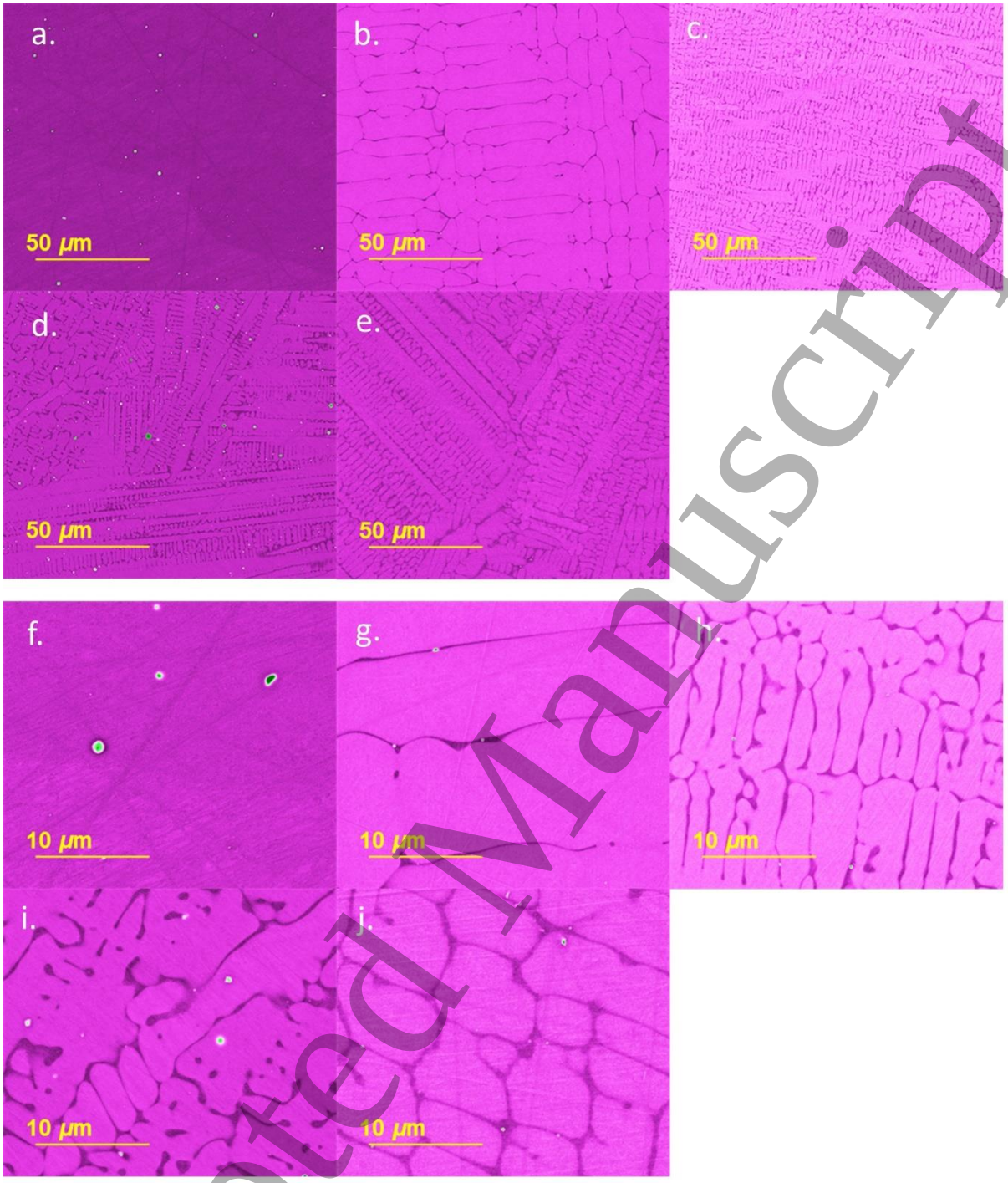

Figure 3. 2,000x zoom false colour ("GreenPinkTones") images of a. CFN-$Cr_{1.0}Cu_{0.0}$, b. CFN-$Cr_{1.0}Cu_{0.5}$, c. CFN-$Cr_{1.0}Cu_{1.0}$, d. CFN-$Cr_{0.8}Cu_{1.0}$, e. CFN-$Cr_{0.0}Cu_{1.0}$; 10,000x zoom false colour images of f. CFN-$Cr_{1.0}Cu_{0.0}$, g. CFN-$Cr_{1.0}Cu_{0.5}$, h. CFN-$Cr_{1.0}Cu_{1.0}$, i. CFN-$Cr_{0.8}Cu_{1.0}$, and j. CFN-$Cr_{0.0}Cu_{1.0}$

SEM analysis was performed for the compositions CFN-$Cr_{1.0}Cu_{0.5}$, CFN-$Cr_{1.0}Cu_{0.0}$, CFN-$Cr_{1.0}Cu_{1.0}$, CFN-$Cr_{0.8}Cu_{1.0}$, and CFN-$Cr_{0.0}Cu_{1.0}$ (Figures 3). False colour was applied to the

obtained micrographs in Mathematica to better observe the microstructural changes. Micrographs of 2,000x and 10,000x zoom are shown in Figures 3 a-e and 3 f-i respectively. For the CFN-$Cr_{1.0}Cu_{0.0}$ alloy, there appears to be no segregation within the matrix but some precipitates within the matrix may be observed (green in the micrographs) that have been determined through EDX to be Cr-rich. The microstructure appears to consist of a solid solution as reported in literature and is in agreement with the XRD traces shown here. A secondary phase forms with the addition of Cu to the system, and some precipitates are also observed in the other compositions, which may be due to the unhomogenised nature of the as-cast sample. From the micrographs, segregation appears to occur at the grain boundaries; EDX confirms this secondary phase to be Cu-rich. The Cu-rich phase is expected from previous experimental results [20, 23] as well as the analysis of the binary enthalpy of mixing values of the CFN-$Cr_{1.0}Cu_{1.0}$ system (Figure 2). As the Cu-containing binary enthalpy of mixing values are all positive, it is expected that Cu segregates from the system to form the secondary phase. The relative proportion of the secondary phase to the matrix was obtained by considering the pixel level in the micrographs. These results show a decrease in the solid solution area due to Cu segregation on Cu addition to form CFN-$Cr_{1.0}Cu_{0.5}$ (96.2%) and CFN-$Cr_{1.0}Cu_{1.0}$ (87.2%), which is expected. However, a decrease in the Cu-rich secondary phase area is also observed on Cr reduction for CFN-$Cr_{0.8}Cu_{1.0}$ (matrix area 83.9%) and CFN-$Cr_{0.0}Cu_{1.0}$ (matrix area 64%). This decrease of the Cu-rich phase is not expected as the molar fraction of Cu in the compositions would have increased from 0.2 (in the case of CFN-$Cr_{1.0}Cu_{1.0}$) to 0.21 (for CFN-$Cr_{0.8}Cu_{1.0}$) and 0.25 (for CFN-$Cr_{0.0}Cu_{1.0}$). Thus, the volume fraction of the Cu-rich phase increases with Cu increase in CFN-$Cr_{1.0}Cu_{0.0}$, but decreases on Cr reduction from CFN-$Cr_{1.0}Cu_{1.0}$.

3.3 Magnetic Properties

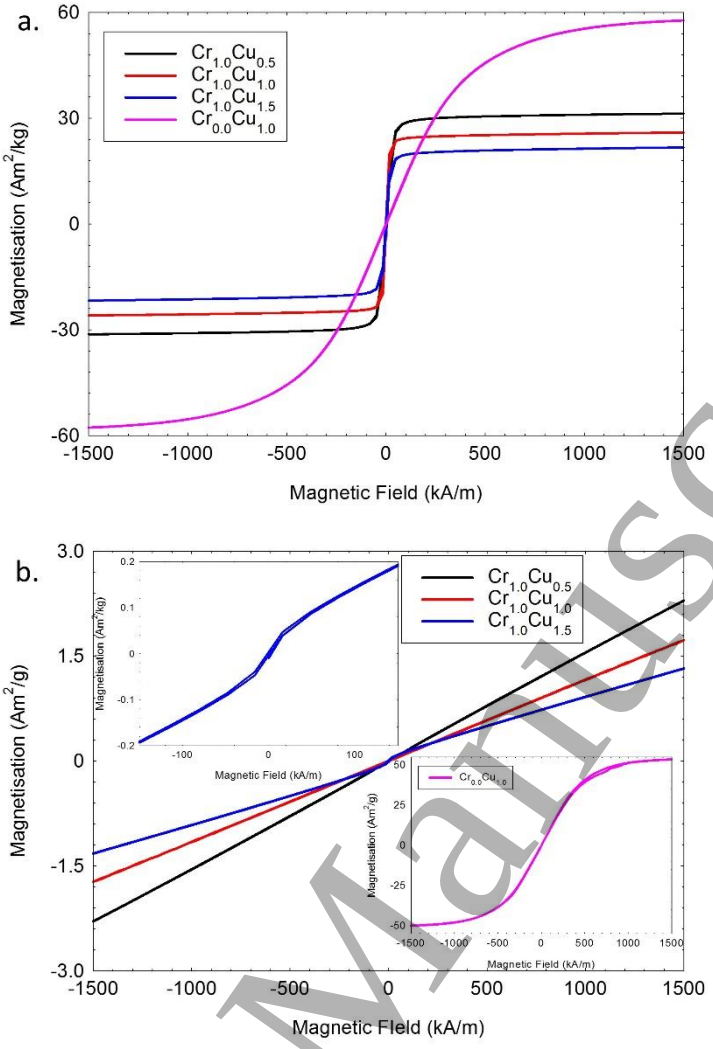

Figure 4. Magnetisation hysteresis loops taken at a) 10 K, and b) 300 K for the CFN-$Cr_{1.0}Cu_x$ and CFN-$Cr_{0.0}Cu_{1.0}$ alloys, inset b: M-H loops for CFN-$Cr_{0.0}Cu_{1.0}$ sample (lower) and CFN-$Cr_{1.0}Cu_{1.5}$ (upper)

The magnetic hysteresis loops of the alloys are given in Figure 4. The addition of Cu to the base alloy CFN-$Cr_{1.0}Cu_{0.0}$ reduces the saturation magnetisation at 10 K (Figure 4a), but does not change the shape of the magnetisation hysteresis loop. In contrast, addition of Cr to the CFN-$Cr_{0.0}Cu_{1.0}$ alloy does change the magnetisation hysteresis loop shape. The Cr addition also reduces the anisotropy field (H_k) from ~ 1350 kA/m for CFN-$Cr_{0.0}Cu_{1.0}$ to ~ 134 kA/m for CFN-$Cr_{1.0}Cu_{1.0}$. Thus the Cr dominates the soft magnetic properties of the HEA compared to Cu. The coercive fields (H_c) for all the alloys studied were less than 2 kA/m, so are counted as soft magnetic materials.

At 300 K (Figure 4b), all the samples containing Cr were paramagnetic, while the sample without Cr, CFN-$Cr_{0.0}Cu_{1.0}$ is magnetic. For the CFN-$Cr_{1.0}Cu_{1.5}$ sample, the paramagnetic phase dominates the signal, but a small hysteresis loop can be observed at fields close to zero (*cf.* upper inset in Figure 4b). Subtracting the paramagnetic contribution away from the total magnetisation gives a small magnetic hysteresis loop, with saturation magnetisation of 0.097 Am^2/kg. This shows both paramagnetic and ferromagnetic behaviours, which further supports the formation of two FCC phases as indicated in our XRD and neutron diffraction data (Figure 1) and Dahlborg *et al* [21] CFN-$Cr_{1.0}Cu_{1.5}$ structural data.

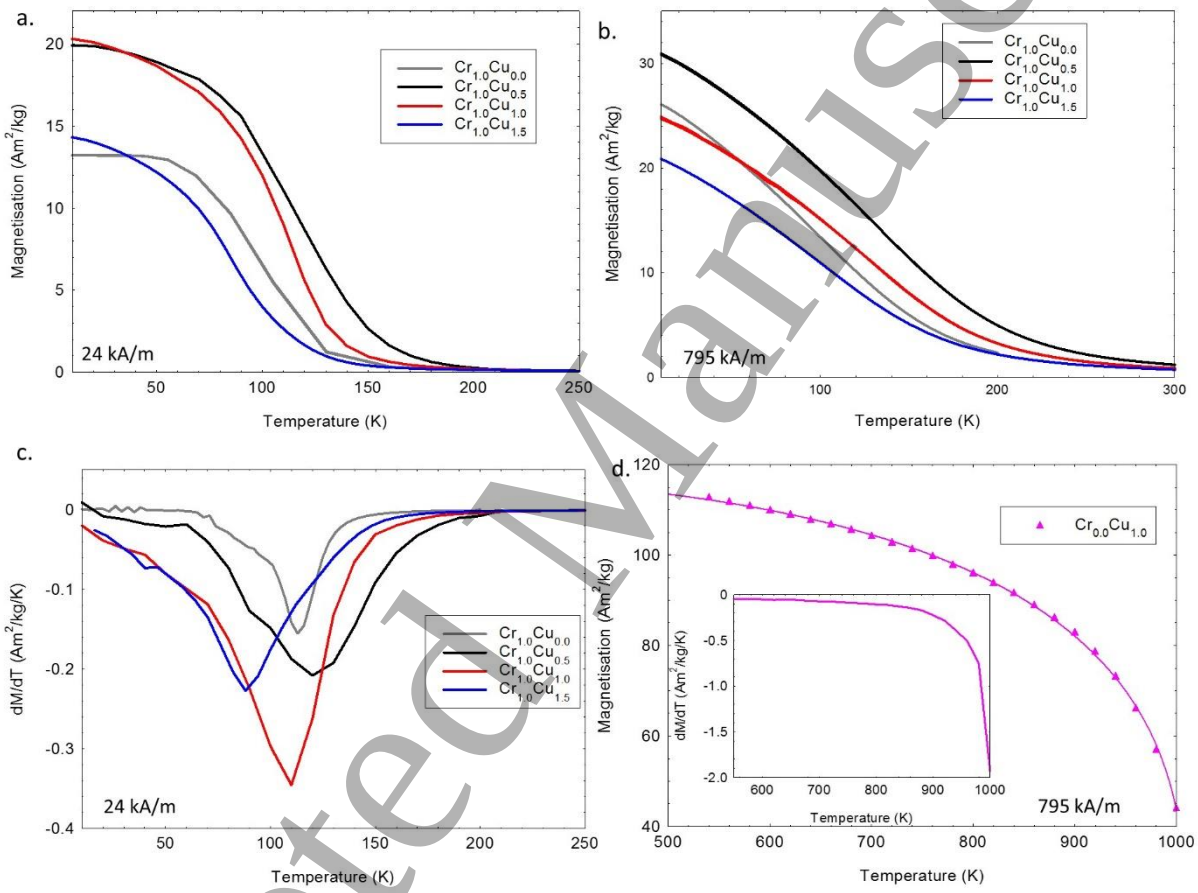

Figure 5. Magnetisation as a function of temperature for the CFN-$Cr_{1.0}Cu_x$ alloys at applied fields of 5a. 24 kA/m. 5b 795 kA/m. 5c dM/dT as a function of temperature below 300 K for an applied field of 24 kA/m for the CFN-$Cr_{1.0}Cu_x$ alloys. 5d. Magnetisation as a function of temperature above 500 K at applied field of 795 kA/m for the CFN-$Cr_{0.0}Cu_{1.0}$ alloy. The solid line is a Bloch fit to the data. Inset: dM/dT as a function of temperature above 300 K.

The magnetisation as a function of temperature (*M-T*) was measured at two applied fields, 24 kA/m and 795 kA/m. The difference in the *M-T* data between the two fields (Figures 5a and

5b), is due to the shape of the hysteresis loops for the different CFN-$Cr_{1.0}Cu_x$ alloys. The addition of Cu to CFN-$Cr_{1.0}Cu_{0.0}$ increased the magnetisation as a function of temperature, with CFN-$Cr_{1.0}Cu_{0.5}$ having the largest magnetisation for the CFN-$Cr_{1.0}Cu_x$ alloys. Here the *dM/dT* data in Figure 5c, was used to determine the Curie temperature, which corresponds to the "peak" in the *dM/dT* plot. The data presented are for the 24 kA/m applied field, as the sharper transition, provides a more accurate measurement. HEAs [25] seem to have wider temperature ranges (~100 K) for the transition from paramagnetic to ferromagnetic compared to traditional magnetic alloys (~10 K). This means that using the *dM/dT* method to determine the Curie temperature can lead to lower values than expected, as above this temperature the magnetisation hysteresis loop will contain both a ferromagnetic and paramagnetic component. The saturation magnetisations at 10 K, and the Curie Temperatures are given in Table 2.

The small addition of Cu to CFN-$Cr_{1.0}Cu_{0.0}$ increased the saturation magnetisation and Curie temperature, as the CFN-$Cr_{1.0}Cu_{0.5}$ alloy saturation magnetisation is ~5 Am^2/kg larger than the CFN-$Cr_{1.0}Cu_{0.0}$ alloy's saturation magnetisation and the Curie temperature is 7 K higher (Table 2). This means that although there is an increase in non-magnetic element content in CFN-$Cr_{1.0}Cu_{0.5}$ (34%) compared to CFN-$Cr_{1.0}Cu_{0.0}$ (25%), the reduction in the Cr composition (25% in CFN-$Cr_{1.0}Cu_{0.0}$ compared to 22% in CFN-$Cr_{1.0}Cu_{0.5}$), is enough to increase both the saturation magnetisation and the Curie temperature. The CFN-$Cr_{1.0}Cu_{1.0}$ alloy has the same Curie temperature and saturation magnetisation as the CFN-$Cr_{1.0}Cu_{1.0}$ alloy, but with 40% non-magnetic elements. Thus the addition of Cu did not degrade the magnetic properties of the alloy, rather these properties are dominated by the Cr concentration.

From Figure 5d, it is observed that the sample without Cr (CFN-$Cr_{0.0}Cu_{1.0}$) has a Curie temperature above 1000 K, thus the addition of Cr reduced the Curie temperature by ~ 900 K. For the addition of Cu to CFN-$Cr_{1.0}Cu_{0.0}$, the change in the Curie temperature is much smaller, ~50 K. This means that the Cu concentration can be used to tune the Curie temperature of the alloys across a small temperature range. On the other hand, the Cr concentration can be used to tune the Curie temperature over a much larger temperature range, so allowing the Curie temperature to be moved to around 300 K, and then broaden the working temperature range using Cu, both of which are required for magneto-caloric applications. Kormann *et al.* [26] predicted the Curie Temperature of CFN-$Cr_{1.0}Cu_{0.0}$ to be 156

K, while Lucas *et al.* [15] measured it to be 119 K. This measurement is in good agreement with the Curie temperature we measured for CFN-$Cr_{1.0}Cu_{0.0}$ (T_C = 113 K).

The Curie temperature of the CFN-$Cr_{0.0}Cu_{1.0}$ alloy could not be measured, as the highest temperature for the SQUID is 1000 K. Thus, Bloch Law [27] was fitted to the M *vs.* T data (Figure 5d) to calculate the Curie temperature. It was calculated to be 1012 K, which is higher than the value predicted by Kormann *et al.* [26] of 826 K.

Table 2. Magnetics properties of the CFN-Cr_yCu_x samples. *: Calculated.

Sample	**Saturation Magnetisation, M_s at 10 K and 1590 kA/m (Am^2/kg)**	**Curie temperature, T_c (K)**	**Entropy change at 2T, $-\Delta S_m$ (J/kg/K)**	**Refrigeration capacity (*RC*) at 2T (J/K)**
CFN-$Cr_{1.0}Cu_{0.0}$	26.1	113	0.34	51
CFN-$Cr_{1.0}Cu_{0.5}$	31.4	120	0.36	62
CFN-$Cr_{1.0}Cu_{1.0}$	26	110	0.34	54
CFN-$Cr_{1.0}Cu_{1.5}$	21.8	88	0.27	41
CFN-$Cr_{0.0}Cu_{1.0}$	57.7	1012*	>0.97	-
CFN-$Cr_{0.8}Cu_{1.0}$	37.2/40.8 (rod)	205/223 (rod)	0.34/0.41 (rod)	70/70 (rod)

3.4 Magneto-caloric properties

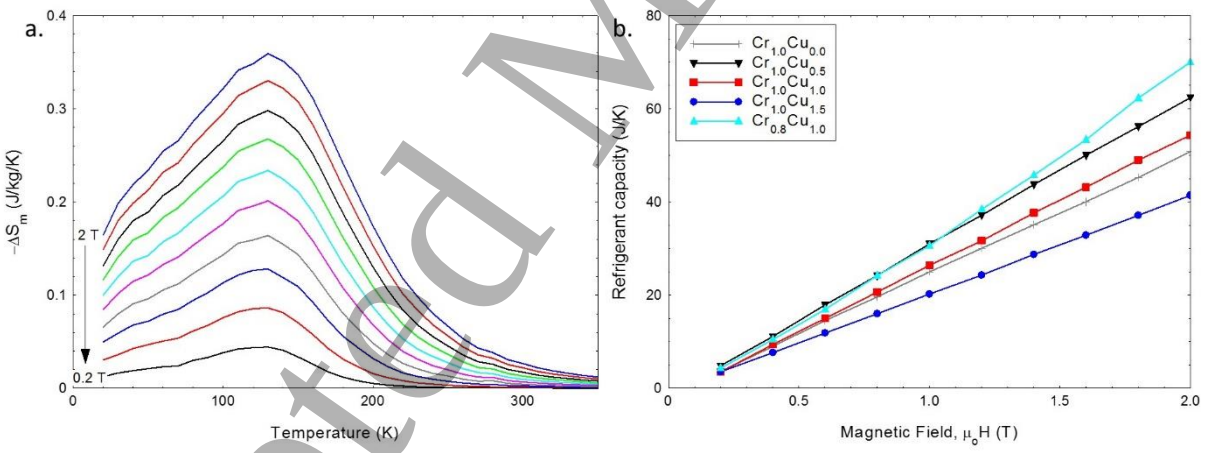

Figure 6a. Change in Entropy as a function of magnetic field (0.2 T steps) and temperature for the CFN-$Cr_{1.0}Cu_{0.5}$ sample. 6b. Refrigeration capacity as a function of magnetic field for the CFN-$Cr_{1.0}Cu_x$ and CFN-$Cr_{0.8}Cu_{1.0}$ samples.

As these HEAs contain only transition metals, it makes them a possible alternative to the rare earth-based alloys for magneto-caloric applications. To determine whether these alloys could be used for magnetic refrigeration, the change in entropy (ΔS) as a function of field (H) and

temperature (*T*) were determined from the first quadrant magnetisation versus field loops using the following equation [28]:

$$\Delta S = -\int_0^H \left(\frac{\delta M(H,T)}{\delta T}\right)_H dH \quad (1)$$

From the change in entropy data (Figure 6a), the refrigeration capacity (*RC*) for each alloy was determined using:

$$RC = \left|\Delta S_{peak}\right| \times \delta T_{FWHM} \quad (2)$$

where ΔS_{peak} is the peak in the ΔS versus temperature curve and δT_{FWHM} is the temperature range at the full width half maximum of the ΔS versus temperature curve (example given for CFN-$Cr_{1.0}Cu_{0.5}$ in Figure 6a). Thus Figure 6b gives the refrigeration capacity for the CFN-$Cr_{1.0}Cu_x$ alloys as a function of applied magnetic field. Due to the Curie temperature of the CFN-$Cr_{0.0}Cu_{1.0}$ alloy being above the temperature range of the SQUID, it was not possible to determine the refrigeration capacity for it.

Lucas *et al.* [15] determined the *RC* for CFN-$Cr_{1.0}Cu_{0.0}$ to be 43 J/kg at 1.5 T, so in good agreement with our data for CFN-$Cr_{1.0}Cu_{0.0}$ (*RC* = 38 J/kg at 1.5 T). From Table 2, it is observed that the addition of Cu to CFN-$Cr_{1.0}Cu_{0.0}$ increases the *RC* for the alloy, along with the Curie temperature. From Figure 5a and 5b, it is observed that the phase transition from paramagnetic to ferromagnetic shows no thermal hysteresis, this means that the transition is a second order transition. Although, first order phase transitions are preferred for magnetic refrigeration applications, due to their higher refrigerant capacity [11, 29], and change in entropy, these materials tend to be brittle during thermal cycling, so have a shorter lifetime, when compared to second order MCE alloys, plus there are loses associated with the thermal hystersis. Hence, although second order MCE materials have lower refrigerant capacity in general, they are likely to last longer in applications, due to their other factors being more favourable. Other advantages of HEAs such as CFN-$Cr_{1.0}Cu_{1.0}$ alloys, are that they contain only transition metal elements, which can make them cheaper and have good wear resistance [21, 22]. Therefore, the superior thermal lifetime and corrosion resistance is likely to balance the reduction in refrigerant capacity in these materials, so still making them attractive for magnetic refrigeration or thermal waste energy harvesting [30].

For any refrigeration application, the magnetic field required for the magneto-caloric effect process, will have to be produced by either a permanent magnet or an electromagnet. Due to the size an electromagnet would have to be, to produce a magnetic field above 1 T, it is likely that permanent magnets will be used. Therefore the most interesting range of the refrigeration capacity is between 1 – 2 T, ideally close to room temperature. Table 3 provides a summary of the magneto-caloric properties for the HEAs in the literature, including the $-\Delta S$ and *RC*. From table 3, there are a number of points to be observed, the first is that all the HEAs that contain Co and Cr have $-\Delta S$ less than 1. Note that the two HEAs with $-\Delta S$ greater than 1, which contain no rare earth elements are based on NiMnSi [33, 34], which is a Heusler alloy and the entropy change is due to a magneto-structural transition. The HEAs with only rare-earth elements, have the largest *RC* at 2 T, but the peak temperature is lower than 200 K. The second point to note is for CoFeNiCr based alloys, the highest *RC* measured at 2T is ~80 J/K. Even the FeNiMnGeSi alloy [33], which has the largest $-\Delta S$ by a factor 10 has a smaller *RC* compared to CoFeNiCr based alloys, due to the narrow temperature range of the $-\Delta S$ peak. This means that there is a balance between the magnitude of the $-\Delta S$ and the temperature range of the transition. From the data in the table, the 'best' HEA is CoFeNiCuMn [12], exhibiting the highest RC for the HEA alloys at a modest field of 0.55 T. Another observation is that the reduction or removal of Cr in the alloy increases $-\Delta S$, peak temperature T_{peak} and *RC,* suggesting that Cr is detrimental to magneto-caloric properties. This is observed for our CFN-$Cr_{0.0}Cu_{1.0}$ sample, which had the largest $-\Delta S$ for our alloys, but also a T_{peak} greater than 1000 K. The T_{peak} and $-\Delta S$ for our CFN-$Cr_{1.0}Cu_{0.0}$ sample is in good agreement with those in the literature [14, 15]. Also the reduction of Cr in CFN- $Cr_{0.8}Cu_{1.0}$ gives a competitive $-\Delta S$ and *RC* for CoFeNiCr based HEAs. For the traditional magneto-caloric materials, such as $LaFe_{11.6}Si_{1.4}$ and MnAs, the Curie temperature also has to be tuned using dopants such as Co, H and Si, which moves the T_c to around 280 – 300 K, but this decreases the refrigerant capacity. At 2 T, the refrigerant capacity of $LaFe_{11.6}Si_{1.4}$ is in the range 100 – 150 J/K [11, 29, 31] for a temperature range between 180 – 220 K and for $MnFeP_{1-x}As_x$ is in the range 200 - 250 J/K [11, 32] for a temperature range 260 - 340 K. Thus they are higher than those measured for the HEAs, but have the disadvantages mentioned above, meaning the search for new materials is still ongoing, and HEAs may hold the key in the long run.

Table 3. Summary of the magneto-caloric properties of HEAs from the literature.

Alloy	**Entropy change*, $-\Delta S_m$ (J/kg/K)**	**T_{peak} (K)**	**RC* (J/K)**
$CoFeNiCr_{1.0}Cu_{0.0}$ (this work)	0.34 (2 T)	110	51 (2 T)
$CoFeNiCr_{1.0}Cu_{0.5}$ (this work)	0.36 (2 T)	130	62 (2 T)
$CoFeNiCr_{1.0}Cu_{1.0}$ (this work)	0.34 (2 T)	120	54 (2 T)
$CoFeNiCr_{0.8}Cu_{1.0}$ (this work)	0.4 (2 T)	220	70 (2 T)
$CoFeNiCr_{0.0}Cu_{1.0}$ (this work)	>0.97 (2 T)	>1000	-
$CoFeNi_{0.5}Cr_{0.5}$ [17]	0.56 (2 T)	270	75.6 (2 T)
$CoFeNi_{0.5}Cr_{0.5}Al$[17]	0.4 (2 T)	685	62 (2 T)
CoFeNiCr [15]	0.27 (1.5 T) 0.35 (2 T)	100 100	43 (1.5 T) -
CoFeNiCrAl [16]	0.31 (3 T)	290	119.2 (3 T)
$CoFeNi_{1.5}Cr_{0.5}Al$ [16]	0.28 (2 T)	150	-
CoFeNiCr [14]	0.75 (5 T)	100	~50 (2 T)
$CoFeNiCrPd_{0.25}$ [14]	0.9 (5 T)	225	63 (2 T)
CoFeNiCuMn [12]	0.8 (0.55 T)	400	~112[a] (0.55 T)
$CoFeNiCu_{0.95}Mn_{1.05}$ [12]	0.45 (0.55 T)	280	-
$CoFeNiCu_{0.9}Mn_{1.0}$ [12]	0.4 (0.55 T)	265	-
$FeNiMnGe_{0.8}Si_{0.8}$ [33]	7.3 (2.5 T) 5.4 (2 T)	143 143	~51[a] (2.5 T) ~38[a] (2 T)
$Fe_{26.7}Ni_{26.7}Mn_{20}Ga_{15.6}Si_{11}$ [34] (annealed at 700 K)	1.59 (2 T)	334	75.68 (2 T)
$Fe_{26.7}Ni_{26.7}Mn_{20}Ga_{15.6}Si_{11}$ [34] (as-cast)	0.64 (2T)	315	29.04 (2 T)
GdDyErHoTb [35]	8.6 (5T) ~2.5 (2 T)	186	627 (5 T) ~250 (2 T)
GdErHoTb [35]	4.8 (5 T)	139	137 (5 T)
DyErHoTb [35]	0.65 (5 T)	52	27.3 (5 T)

* The applied field for the entropy change and *RC* is given in the brackets; [a] estimated from the data provided in the paper

The compositions listed here can be further characterised according to their enthalpy of mixing (ΔH) using the sub-regular solid solution model [36] to evaluate the binary enthalpy of mixing values [36]. Two main contributors to the magneto-caloric properties of HEAs may be expected: 1) For near-ideal solid solutions where the enthalpy of mixing is close to zero, the unit cell's sites are randomly occupied and can lead to spin driven ordering such as in [38]; 2)

At highly negative enthalpies of mixing, the solid solution structure is increasingly metastable below a critical temperature due to compositional fluctuations. These structural changes at highly negative enthalpy of mixing values (from –20 kJ/mol onwards) are observed for the FeNiMnGeSi and FeNiMnGaSi-type compositions, which are in agreement with this hypothesis. This is illustrated in Figure 7.

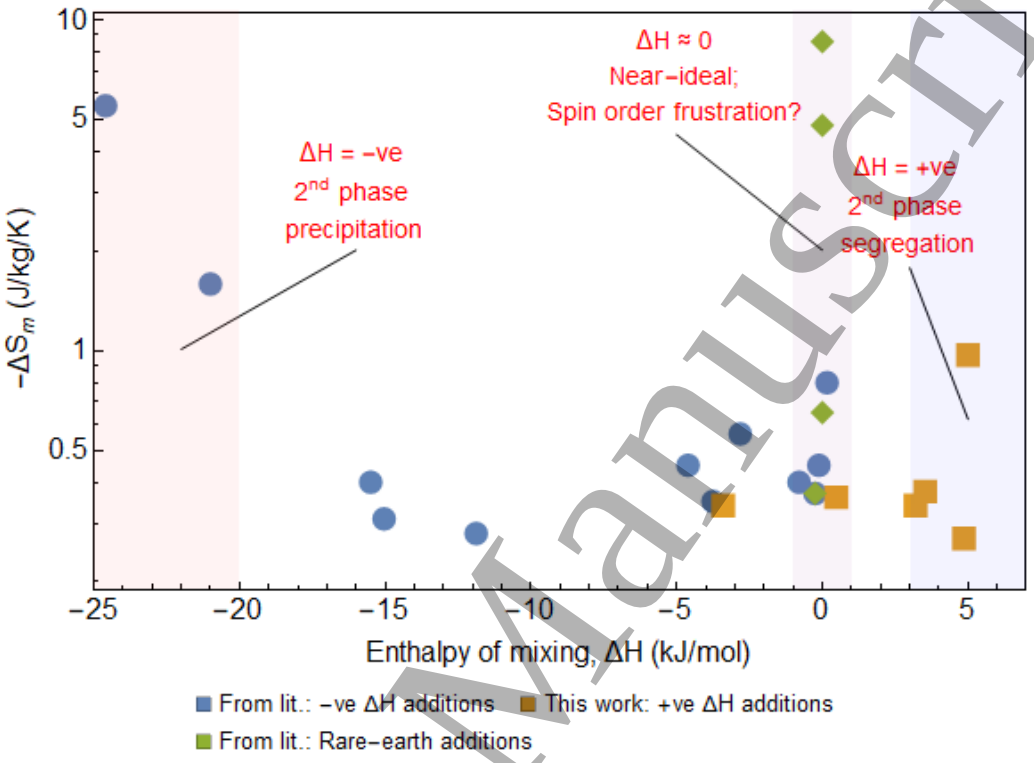

Figure 7. Plot of the entropy change (2T) against the enthalpy of mixing.

The plot shows the values of various HEAs (rare-earth and none rare-earth) compositions listed in Table 3. Previous experimental studies have not considered the effect of large Cu addition on the magneto-caloric properties of the structure. Similarly to Ti, V, or Al [39] Cu does stay in a solid solution with other transition metals – it possesses a highly positive enthalpy of mixing, which leads to Cu segregation and the formation of a segregated structure – this has been confirmed in high-resolution structural characterisations where multiple FCC peaks are resolved for Cu-containing HEAs [20]. Other work has shown the coexistence of other alloy elements with the segregated Cu in CoCrFeNiCu-type compositions. An increase in temperature may affect the miscibility of the atoms due to entropic contributions and may be responsible for the increased magnetic entropy change for the Cu compositions. It can be seen from Figure 7 that when the enthalpy of mixing is increased for the CoFeNiCu

composition, the magnetic entropy increases so that it is comparable to the previously reported $CoCrFeNiPd_{0.25}$ composition. Finally, for near-ideal compositions, which have enthalpy of mixing values close to zero (0 +/- 0.5 kJ/mol) and where no particular precipitation or segregation is likely to occur, high magnetic entropy values are seen. For example, high magnetic entropy values were reported for the rare-earth containing compositions, which have enthalpy of mixing values of zero with each other (*i.e.* Tb, Dy, Ho, Gd, and Er) [35]. Thus, it appears that if a material with high magnetic entropy is desired, then the alloy should have one of the following three properties while maintaining the appropriate trade-offs with the other properties: 1) Enthalpy of mixing close to zero (i.e. near-ideality of the solid solution), 2) highly negative enthalpy of mixing values below a critical metastable temperature, or 3) Maximum segregation. Although additional competing contributions can affect overall magneto-caloric properties, the three property criteria identified here can serve as a good first pass for magneto-caloric alloy design. Of these, the latter has not been fully explored and may be a way to fabricate cost-effective magneto-caloric materials.

3.5 Effect of synthesis conditions on properties

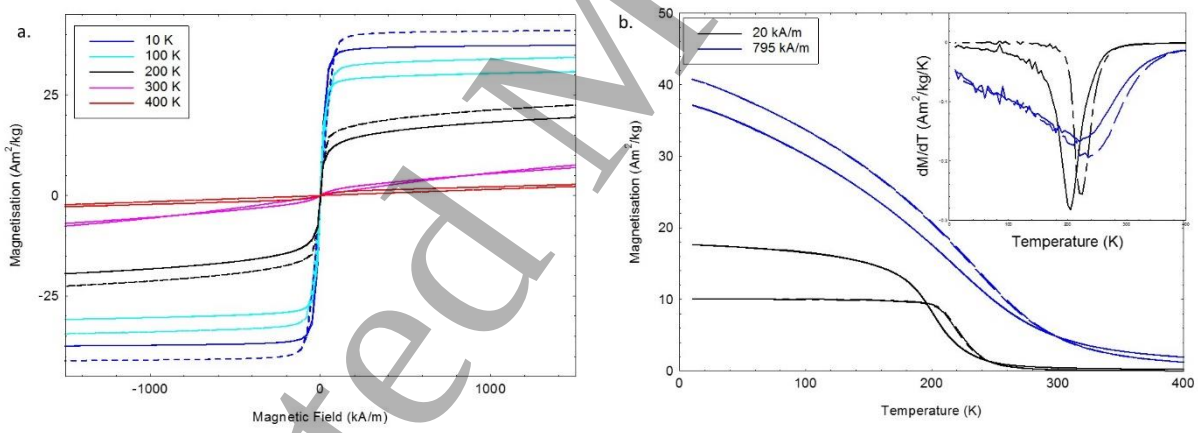

Figure 8a. Magnetisation as a function of magnetic field and temperature for the CFN-$Cr_{0.8}Cu_{1.0.}$ For the arc-melted ingot (solid line) and suction-cast rod (dashed line) samples. 8b. Magnetisation as a function of temperature for both CFN-$Cr_{0.8}Cu_{1.0}$sample at 24 kA/m and 795 kA/m. Inset: dM/dT as a function of temperature for the CFN-$Cr_{0.8}Cu_{1.0}$ sample at 24 kA/m and 795 kA/m. The solid lines are for the arc-melted ingot sample and the dashed lines are for the suction cast rod sample.

If it is roughly assumed that the Curie temperature is proportional to the amount of Cr within the alloy, then, to achieve a Curie temperature of around 300 K, then the ratio of Cr to Cu added to CFN should be 0.8:1.0. To test this hypothesis another sample was arc-melted into an ingot followed by suction casting into a rod with the nominal composition of CFN-$Cr_{0.8}Cu_{1.0}$. To determine whether the suction casting into a rod made a difference to the magnetic properties, both the as-cast arc melted ingot and the suction cast rod were studied. As expected, the alloy was FCC (Figure 1b and Table 1). The temperature and field dependence magnetisations were measured. Figure 8a shows the magnetisation hysteresis loops as a function of temperature for both samples. It is observed there is a difference in both the shape of the magnetisation hysteresis loop and the saturation magnetisation magnitude between the two synthesis processes. It is also observed that the arc-melted sample was still magnetic at room temperature, but there is a large paramagnetic component observed at the higher fields, while the rod was fully paramagnetic (Figure 8a). The saturation magnetisation at 300 K, and 1590 kA/m was 7.2 Am^2/kg, which is a factor of 8 smaller than the CFN-$Cr_{0.0}Cu_{1.0}$ sample containing no Cr, but a factor of 7 larger than the CFN-$Cr_{1.0}Cu_{1.0}$ sample at 300 K, as the CFN-$Cr_{0.8}Cu_{1.0}$ sample still had a small magnetic component, while the CFN-$Cr_{1.0}Cu_{1.0}$ sample was purely paramagnetic. Thus reducing the Cr has increased both the room temperature magnetisation, and the 10 K saturation magnetisation (Table 2), to be larger than all the CFN-$Cr_{1.0}Cu_x$ alloys' magnetisations. The Curie temperature was determined from the *dM/dT* plot to be 205 K for the arc-melted ingot and 223 K for the rod (Figure 8b inset), so an increase for the suction cast rod, but the temperature transition range is reduced. Similar to other HEAs studied [25], the temperature transition range for both samples is over a 100 K, meaning that there is still a small magnetic component at 300 K. The Curie temperature for the CFN-$Cr_{0.8}Cu_{1.0}$ rod is 113 K higher than the CFN-$Cr_{1.0}Cu_{1.0}$ alloy, thus as expected reducing the Cr has increased the Curie temperature.

The magneto-caloric data were taken for both samples and the refrigeration capacity was plotted on the same plot as the other four alloys (Figure 6b) to allow comparison. It is observed that at 2 T, the refrigerant capacity is 70 J/K for both synthesis methods, which is higher than the other alloys, again showing that reducing the Cr improves the magnetic properties.

Generally, the $-\Delta S_m$ peak values increase with decreasing T_C in similar systems. However, the $-\Delta S_m$ values decrease with decreasing T_C in the CFN-$Cr_{1.0}Cu_{1.0}$ systems, which is similar to some reported systems, *i.e*. $Mn_5Ge_{3-x}Si$ [39] and $MnAs_{1-x}Sb$ [7]. Taking CFN-$Cr_{1.0}Cu_{0.0}$ as reference, the $M_S\backslash S_M$ changes by 0.2\0.05 (CFN-$Cr_{1.0}Cu_{0.5}$), 0\0 (CFN-$Cr_{1.0}Cu_{1.0}$), and -0.16\-0.21 (CFN-$Cr_{1.0}Cu_{1.5}$). This suggests that in CFN-$Cr_{1.0}Cu_{0.5}$ the increase in magnetisation does not completely influence $-\Delta S_m$ values in comparison to the other compositions. This can be further studied by analysing the ratio of the non-ferromagnetic binary pairs (unpaired Cu, and Cr-Cu) for the compositions studied here, which are 0, 0.22, 0.34, and 0.43 (for CFN-$Cr_{1.0}Cu_{0.0}$, CFN-$Cr_{1.0}Cu_{0.5}$, CFN-$Cr_{1.0}Cu_{1.0}$, and CFN-$Cr_{1.0}Cu_{1.5}$ respectively). Based on the dilution of the ferromagnetic elements, it would be reasonable to assume that the magnetisation decreases with respect to this. However, the experimental results show that the saturation magnetisation is maximum for CFN-$Cr_{1.0}Cu_{0.5}$ (31.4 Am^2/kg).

The magnetic FCC lattice (inferred to be CFN-$Cr_{1.0}Cu_{0.0}$ from SEM and XRD analysis) is likely to be randomly occupied, as the CFN-$Cr_{1.0}Cu_{0.0}$ enthalpy of mixing evaluated using the sub-regular solution model is near-ideal (-3 kJ/mol). Thus these components constitute the main phase, *i.e* the Cu-poor matrix regions, which contribute the most magnetically. When the magnetically important *3d* electrons of adjacent atoms are relatively close to each other, the exchange interaction is negative, but when they are further away, the exchange interaction becomes positive before slowly dropping off [39, 40] – this is represented by the well-known Slater relation [41]. A variation of interatomic Cr distances and its position in the unit cell due to Cu addition and the resulting elemental re-segregation may therefore change the exchange interaction [41-43]. Some antiferromagnetic interactions may occur, which may affect the magnetic ordering behaviour near T_c. The Slater-Pauling curve has been reconstructed in Figure 9b for the 3d transition elements. Cr addition to form CoCr and NiCr alloys are known to shift the compositions in this curve below the Bethe-Slater curve; similar behaviour is observed in the alloys synthesised here. Figure 9a shows the temperature dependence of the AC susceptibility obtained from ZFC experiments dips at temperature below T_C with increasing Cu content, which shows the effect of magnetic ordering [44]. This is counterintuitive as the ratio of Co-Cr-Fe-Ni is constant across all the compositions.

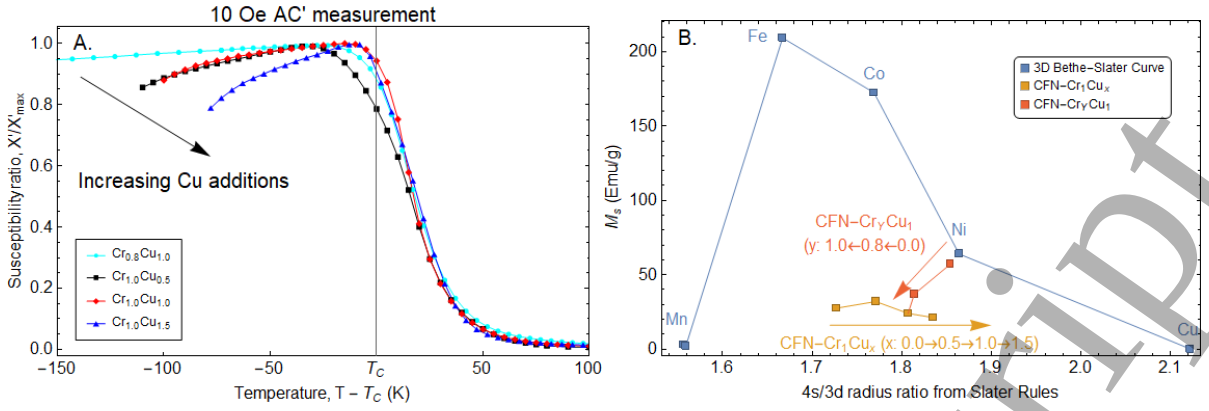

Figure 9a. AC measurements (X') of CFN-$Cr_{1.0}Cu_x$ and CFN-$Cr_{0.8}Cu_{1.0}$ sample with T_C < 300K. For easier comparison, the data has been scaled against respective T_C values on the x-axis and respective X'_{max} values on the y-axis. 9b. Position of the CoFeNi-Cr_YCu_X compositions with respect to a reconstructed Bethe-Slater curve using Slater rules [40].

In some systems, changes to the unit cell size influences the nature of the magnetic ordering. In order to gain more information on the local environment of atoms in the CFN-$Cr_{1.0}Cu_{0.0}$ matrix, Wigner-Seitz cell calculations were performed by approximation of the volume *per* unit atom ratios from the FCC cell parameters obtained *via* XRD diffraction (Table 1). Increasing Cu addition to the CFN-$Cr_{1.0}Cu_x$ composition increases the Wigner-Seitz radius from 1.3971 to 1.4026, 1.4034, and 1.4053 Å (*x*: 0, 0.5, 1, and 1.5). The reduction in Cr changes the Wigner-Seitz radius from 1.4034 to 1.4006 and 1.4013 Å (*y*: 1, 0.8, and 0). The fluctuations here with respect to M_s suggests that lattice expansion is not the underlying cause of the M_s increase for CFN-$Cr_{1.0}Cu_{0.5}$ unlike the $CoFeCr_{0.5}Ni_{0.5}$-Al_x alloy systems [25], which disproves the hypothesis of unit cell size influence on magnetisation. Chaudhary *et al.* [44] reported on Ni uptake in the Cu segregated phase in CoCrFeNi-Cu_x compositions on increasing Cu addition. The continual increase in T_C with Cu addition suggests that the Ni concentration in the Cu segregated phase increase with additional Cu addition. From this it may be inferred that diamagnetic Cu interacts with Ni, which results in a change in its oxidation state [45], which may explain why the change in magnetisation is not consistent with the increase in the Wigner-Seitz radius with increase Cu additions. The Ni addition also increases Cr concentration in the CoCrFeNi matrix, which explains the changes in the magnetic ordering in the system.

4. Conclusions

A series of CFN-Cr_yCu_x alloys were fabricated and characterised to understand how the different percentages of Cr and Cu changed the magnetic properties, including the magneto-caloric effect. It was found that the addition of Cr to CFN-$Cr_{0.0}Cu_{1.0}$ decreased the saturation magnetisation at 10 K, the Curie temperature and the magneto-caloric effect. For CFN-$Cr_{0.0}Cu_{1.0}$, the Curie temperature was calculated to be 1012 K, which was over 900 K higher than the CFN-$Cr_{1.0}Cu_{1.0}$ Curie temperature. Cu addition to CFN-$Cr_{1.0}Cu_{0.0}$ to form CFN-$Cr_{1.0}Cu_{0.5}$ improved the saturation magnetisation and Curie temperature. Comparing the T_{peak} and refrigeration capacity data for the different Cr and Cu ratios, a reduction in Cr is required to achieve T_{peak} around 300 K, while the addition of Cu causes segregation in the alloy, which helps to increase the $-\Delta S$. The results show that a CFN-Cr_yCu_x composition (where y is between 0.8 and 0.5 and x is between 0.5 and 1) would provide a broad temperature region for the refrigeration to occur over, with less than 25% change in the refrigeration capacity. This opens up new possibilities for magnetic refrigeration and thermal energy harvesting.

Acknowledgements

This work was supported by the Royal Society Mid-Career Leverhulme Trust Fellowship scheme (SRF\R1\180020) and the Leverhulme Trust (RPG-2018-324). The samples have been prepared within the FP7 European project AccMet NMP4-LA-2011-263206. We wish to acknowledge the Henry Royce Institute for Advanced Materials, funded through EPSRC grants EP/R00661X/1, EP/S019367/1, EP/P02470X/1 and EP/P025285/1 for access to the MPMS-3 SQUID within the Royce at the University of Sheffield. ZYL would like to thank Dr. Pratik Desai for his useful discussions on Cu transition states and magnetisation.

CRediT author statement

JH: Methodology, Investigation, Validation, Formal Analysis, Writing – Original, Writing – Review

ZYL: Conceptualisation, Methodology, Validation, Formal Analysis, Writing – Original, Writing – Review

PG: Investigation, Writing – Review

JC: Investigation, Writing – Review

CP: Investigation, Writing – Review

TH: Investigation, Writing – Review

AQ: Writing – Review

RR: Supervision, Project Administration, Writing – Review

UD: Investigation, Writing – Review

MC: Investigation, Writing – Review

RG: Supervision, Funding Acquisition, Project Administration, Writing – Review

MR: Supervision, Funding Acquisition, Writing – Review

NM: Conceptualisation, Methodology, Supervision, Formal Analysis, Funding Acquisition, Project Administration, Writing – Original

References

[1] European Commission. “An EU strategy on heating and cooling 2016”. *Journal of Chemical Information and Modelling*, 53(9), 1689–1699. (2016) https://doi.org/10.1017/CBO9781107415324.004

[2] "Energy Flow Charts", Flowcharts.llnl.gov, (2019). [Online]. https://flowcharts.llnl.gov/commodities/energy.

[3] Energy Information Administration. “International Energy Outlook”. *Outlook,* 0484 (July), 70–99. (2019) https://doi.org/https://www.eia.gov/outlooks/ieo/pdf/ieo2019.pdf

[4] "What’s so attractive about magnetic refrigeration?" *CIBSE Journal*, (2019). [Online]. https://www.cibsejournal.com/technical/the-appeal-of-magnetic-refrigeration

[5] Chen Y.F., Wang F., Shen B.G,. Hu F.X., Cheng Z.H., Wang G.J., Sun J.R. “Large magnetic entropy change near room temperature in the $LaFe_{11.5}Si_{1.5}H_{1.3}$ interstitial compound”. *Chinese Phys,* 11(2). 741-742 (2002).

[6]. Hu, F. X., Shen, B. G., Sun, J. R., Wang, G. J., & Cheng, Z. H. “Very large magnetic entropy change near room temperature in LaFe 11.2Co0.7Si1.1.” *Appl. Phys. Letts*, 80(5), 826–828, (2002). https://doi.org/10.1063/1.1447592

[7] Wada, H., & Tanabe, Y. “Giant magnetocaloric effect of $MnAs_{1-x}Sb_x$.” *Appl. Phys. Letts*, 79(20), 3302–3304, (2001). https://doi.org/10.1063/1.1419048

[8] Balli, M., Fruchart, D., Gignoux, D., Tobola, J., Hill, E. K., Wolfers, P., and Zach, R. “Magnetocaloric effect in ternary metal phosphides $(Fe_{1-x}Ni_x)2P$”, *J. Magn. Magn. Mats*, 316(2 SPEC. ISS.), 358–360, (2007). https://doi.org/10.1016/j.jmmm.2007.03.018

[9] Planes, A., Mãosa, L., and Acet, M. “Magnetocaloric effect and its relation to shape-memory properties in ferromagnetic Heusler alloys”. *Journal of Physics Condensed Matter*, 21(23), (2009). https://doi.org/10.1088/0953-8984/21/23/233201

[10] Phan, M. H., and Yu, S. C. “Review of the magnetocaloric effect in manganite materials.” *J Magn. Magn. Mat.*, 308(2), 325– 340 (2007). https://doi.org/10.1016/j.jmmm.2006.07.025

[11] Gutfleisch, O., Willard, M. A., Brück, E., Chen, C. H., Sankar, S. G., and Liu, J. P. "Magnetic materials and devices for the 21st century: Stronger, lighter, and more energy efficient." *Advanced Materials*, 23(7), 821–842, (2011). https://doi.org/10.1002/adma.201002180

[12] Kurniawan, M., Perrin, A., Xu, P., Keylin, V., and McHenry, M. "Curie Temperature Engineering in High Entropy Alloys for Magnetocaloric Applications", *IEEE Magnetics Letters*, 7, 610500, (2016), https://doi.org/10.1109/LMAG.2016.2592462

[13] Calvo-Dahlborg, M., Dahlborg, U., Brown, S.G.R. and Juraszek. J., "Influence of the electronic polymorphism of Ni on the classification and design of high entropy alloys." *J. Alloys Compd,* 824, 153895, (2020). https://doi.org/10.1016/j.jallcom.2020.153895

[14] Belyea, D.D., Lucas. M.S., Michel. E., Horwath. J., and Miller. C.W., "Tunable magnetocaloric effect in transition metal alloys", *Scientific Reports*, 5, 15755, (2015), https://doi.org/10.1038/srep15755

[15] Lucas, M. S., Belyea, D., Bauer, C., Bryant, N., Michel, E., Turgut, Z., Leontsev, S. O., Horwath, J., Semiatin, S. L., McHenry, M. E. and Miller, C. W., "Thermomagnetic analysis of $FeCoCr_xNi$ alloys: Magnetic entropy of high-entropy alloys", *J. Appl. Phys*, 113, 17A923, (2013), http://dx.doi.org/10.1063/1.4798340

[16] Na, S-M., Lambert, P.K., Kim, H., Paglione, J. and Jones, N.J, "Thermomagnetic properties and magnetocaloric effect of FeCoNiCrAl-type high entropy alloys", *AIP Advances*, 9, 035010, (2019), https://doi.org/10.1063/1.5079394

[17] Quintana-Nedelcos, A., Leong, Z., and Morley, N. A., "Study of dual-phase functionalisation of NiCoFeCr-Al_x multicomponent alloys for the enhancement of magnetic properties and magneto-caloric effect." *Materials Today Energy,* 20, 100621, (2021), https://doi.org/10.1016/j.mtener.2020.100621

[18] Praveen, S., Murty, B.S., and Kottada, R.S, "Alloying behaviour in multi-component AlCoCrCuFe and NiCoCrCuFe high entropy alloys", *Materials Science and Engineering: A*, 534, 83-89, (2012), https://doi.org/10.1016/j.msea.2011.11.044

[19] Guo, S., Ng, C., Wang, Z., and Liu, C.T. "Solid solutioning in equiatomic alloys: Limit set by topological instability", *J. Alloys Compd*, 583, 410-413, (2014), https://doi.org/10.1016/j.jallcom.2013.08.213

[20] Dahlborg, U., Cornide, J., Calvo-Dahlborg, M., Hansen, T.C., Leong, Z., Asensio Dominguez, L., Chambreland, S., Cuncliffe, A., Goodall, R. and Todd, I. "Crystalline Structures of Some High Entropy Alloy Obtained by Neutron and X-ray Diffraction", *Acta Physica Polonica A*, 128, 4, 552-556 (2015). https://doi.org/10.12693/APhysPolA.128.552

[21] Verma, A., Tarate, P., Abhyankar, A.C., Mohape, M.R., Gowtam, D.S., Deshmukh, V.P., and Shanmugasundaram, T. "High temperature wear in $CoCrFeNiCu_x$ high entropy alloys: The role of Cu", *Scripta Mat.*, 161, 28-31, (2019), https://doi.org/10.1016/j.scriptamat.2018.10.007

[22] Muangtong, P., Rodchanarowan, A., Chaysuwan, D., Chanlek, N., and Goodall, R, " The corrosion behaviour of CoCrFeNi-x (x = Cu, Al, Sn) high entropy alloy systems in chloride solution" *Corrosion Science*, 172, 108740, (2020). https://doi.org/10.1016/j.corsci.2020.108740

[23] Dahlborg, U., Cornide, J.,Calvo-Dahlborg, M., Hansen, T.C., Fitch, A., Leong, Z., Chambreland, S., Goodall, R., "Structure of some CoCrFeNi and CoCrFeNiPd multicomponent HEA alloys by diffraction techniques", *J. Alloys Compd.* 681 330–341, (2016). https://doi.org/10.1016/j.jallcom.2016.04.248.

[24] Zheng, H., Chen, R., Qin, G., Li, X., Su, Y., Ding, H., Guo, J., Fu, H. "Microstructure evolution, Cu segregation and tensile properties of CoCrFeNiCu high entropy alloy during directional solidification," *J. Mater. Sci. Technol*. 38 19–27, (2020). https://doi.org/10.1016/j.jmst.2019.08.019

[25] Morley, N. A., Lim, B. Xi, J., Quintana-Nedelcos, A and Leong, Z. "Magnetic properties of the complex concentrated alloy system $CoFeNi_{0.5}Cr_{0.5}Al_x$", *Scientific Reports*, 10, 14506, (2020), https://doi.org/10.1038/s41598-020-71463-3

[26] Kormann, F., Ma, D., Belya, D. D., Lucas, M. S., Miller, C. W., Grabowski, B., and Sluiter, M. H. F., "Treasure maps for magnetic high entropy alloys from theory and experiment", *Appl. Phys. Letts*, 107, 142404, (2015), http://dx.doi.org/10.1063/1.4932571

[27] Abbas, Q. A, Rodrigues, M., Baco, S., Guan, S and Morley, N. A, "Influence of annealing temperature on the structural and magnetic properties of FeGaSiB thin films", *Thin Solid Films*, 701, 137955, (2020), https://doi.org/10.1016/j.tsf.2020.137955

[28] Quintana-Nedelcos, A., Sanchez Llamazers, J.L., Sanchez-Valdes, C. F., Alvarez Alonson, P., Gorria, P., Shamba, P., and Morley, N. A., "On the correct estimation of the magnetic entropy change across the magneto-structural transition from the Maxwell relation: Study of $MnCoGeB_x$ alloy ribbons," *J. Alloys Compd.*, 694, 1189–1195, (2017). http://dx.doi.org/10.1016/j.jallcom.2016.10.116

[29] Lyubina, J. "Magnetocaloric materials for energy efficient cooling", *J. Phys. D: Appl. Phys.* 50, 053002, (2017), doi:10.1088/1361-6463/50/5/053002

[30] Kishore, R. S. and Priya, S. "A review on design and performance of thermomagnetic devices", *Renew. Sustain. Energy. Rev.* 81, 33-44, (2018), http://doi:10.1016/j.rser.2017.07.035.

[31] Shamba, P., Morley, N. A., Cespedes, O., Reaney, I. M., and Rainforth W. M., "Optimization of magnetocaloric properties of arc-melted and spark plasma sintered $LaFe_{11.6}Si_{1.4}$", *Appl. Phys A*, 122, 732, (2020), doi:10.1007/s00339-016-0253-y

[32] Habiba, U. E., Khattak, K. S., Ali, S. and Khan, Z. H., "MnAs and $MnFeP_{1-x}As_x$ based magnetic refrigerants: a review", *Materials Research Express*, 7, 046106, (2020), https://doi.org/10.1088/2053-1591/ab727c

[33] Law, J. Y., Moreno-Ramírez, L. M., Díaz-García, A., Martín-Cid, A., Kobayashi, S., Kawaguchi, S., Nakamura, T., and Franco, V. "MnFeNiGeSi high-entropy alloy with large magnetocaloric effect", *J. Alloys Compd.*, 855, 1, 157242 (2021), https://doi.org/10.1016/j.jallcom.2020.157424

[34] Sarlar, K,. Tekgül, A. and Kucuk, I., "Magnetocaloric properties in a FeNiGaMnSi high entropy alloy", *Curr. Appl. Phys*. 20, 1, 18-22, (2020), https://doi.org/10.1016/j.cap.2019.09.019

[35] Yuan, Y., Wu, Y., Tong, X., Zhang, H., Wang, H., Liu, X. J., Ma, L., Suo, H. L., and Lu, Z. P., "Rare-earth high-entropy alloys with giant magnetocaloric effect", *Acta Mater.* 125, 481-489, (2017). https://doi.org/10.1016/j.actamat.2016.12.021

[36] Takeuchi, A., and Inoue, A., "Classification of bulk metallic glasses by atomic size difference, heat of mixing and period of constituent elements and its application to characterisation of the main alloying element", *Mat. Trans*. 46, 12, 2817-2829, (2005)

[37] Pakhira, S., Mazumdar, C., Ranganathan, R. and Avdeev, M., "Magnetic frustration induced large magnetocaloric effect in the absence of long range magnetic order", *Scientific Reports*, 7, 7367, (2017). https://doi.org/10.1038/s41598-017-07459-3

[38] Leong, Z., Wrobel, J.S., Dudarev, S. L, Goodall, R., Todd, I. and Nguyen-Manh, D. "The effect of electronic structure on the phases present in high entropy alloys," *Scientific Reports*, &, 39803 (2017). https://doi.org/10.1038/srep39803

[39] Liu, X.B. and Altounian, Z., "Magnetocaloric effect in $Mn_5Ge_{3-x}Si_x$ pseudobinary compounds," *J. Appl. Phys.* 99, 08Q101, (2006). https://doi.org/10.1063/1.2148332.

[40] Slater, J. C., "Atomic Shielding Constants", *Phys. Rev.*, 36, 57, (1930), https://doi.org/10.1103/PhysRev.36.57

[41] Froideval, A., Iglesias, R., Samaras, M., Schuppler, S., Nagel, P., Grolimund, D., Victoria, M. and Hoffelner, W, "Magnetic and Structural Properties of FeCr Alloys", *Phys. Rev. Lett*. 99, 237201, (2007), https://doi.org/10.1103/PhysRevLett.99.237201

[42] Niu, C., Zaddach, A. J., Oni, A. A., Sang, X., Hurt III, J. W., LeBeau, J. M., Koch, C. C. and Irving, D. L., "Spin-driven ordering of Cr in the equiatomic high entropy alloy NiFeCrCo", *Appl. Phys. Lett*, 106, 161906 (2015), https://doi.org/10.1063/1.4918996

[43] Shafranovsky, E. A., Petrov, Yu. I, Gich, M., Racka, K., Slawska-Waniewska, A., Roig, A. and Molins, E., "Structural and magnetic properties of bulk alloys and aerosol nanoparticles in the $Fe_{100-x}Cr_x$ system", *J. Alloys Compd.*, 416, 1-2, 51-57, (2006), https://doi.org/10.1016/j.jallcom.2005.08.046

[44] Chaudhary, V., Soni, V., Gwalani, B., Ramanujan, R. V., and Banerjee, R, "Influence of non-magnetic Cu on enhancing the low temperature magnetic properties and Curie temperature of FeCoNiCrCu(x) high entropy alloys", *Scripta Mat.*, 182, 99-103, (2020), https://doi.org/10.1016/j.scriptamat.2020.02.037

[45] Berdonosov, P.S., Kuznetsova, E. S., and Dolgikh, V. A., "Transition Metal Selenite Halides: A Fascinating Family of Magnetic Compounds", *Crystals*, 8, 4, 159, (2018), https://doi.org/10.3390/cryst8040159